BIOCHEMISTRY
including biophysical chemistry & molecular biology

Article

pubs.acs.org/biochemistry

Why Does Asn71 Deamidate Faster Than Asn15 in the Enzyme Triosephosphate Isomerase? Answers from Microsecond Molecular Dynamics Simulation and QM/MM Free Energy Calculations

Ilke Ugur,[†,‡,§] Antoine Marion,[†,‡] Viktorya Aviyente,[§] and Gerald Monard*[,†,‡]

[†]Université de Lorraine, UMR 7565 SRSMC, Boulevard des Aiguillettes B.P. 70239, F-54506 Vandoeuvre-les-Nancy, France
[‡]CNRS, UMR 7565 SRSMC, Boulevard des Aiguillettes B.P. 70239, F-54506 Vandoeuvre-les-Nancy, France
[§]Department of Chemistry, Boğaziçi University, 34342 Bebek, Istanbul, Turkey

Supporting Information

ABSTRACT: Deamidation is the uncatalyzed process by which asparagine or glutamine can be transformed into aspartic acid or glutamic acid, respectively. In its active homodimeric form, mammalian triosephosphate isomerase (TPI) contains two deamidation sites per monomer. Experimental evidence shows that the primary deamidation site (Asn71-Gly72) deamidates faster than the secondary deamidation site (Asn15-Gly16). To evaluate the factors controlling the rates of these two deamidation sites in TPI, we have performed graphics processing unit-enabled microsecond long molecular dynamics simulations of rabbit TPI. The kinetics of asparagine dipeptide and two deamidation sites in mammalian TPI are also investigated using quantum mechanical/molecular mechanical tools with the umbrella sampling technique. Analysis of the simulations has been performed using independent global and local descriptors that can influence the deamidation rates: desolvation effects, backbone acidity, and side chain conformations. Our findings show that all the descriptors add up to favor the primary deamidation site over the secondary one in mammalian TPI: Asn71 deamidates faster because it is more solvent accessible, the adjacent glycine NH backbone acidity is enhanced, and the Asn side chain has a preferential near attack conformation. The crucial impact of the backbone amide acidity of the adjacent glycine on the deamidation rate is shown by kinetic analysis. Our findings also shed light on the effect of high-order structure on deamidation: the deamidation in a small peptide is favored first because of the higher reactivity of the asparagine residue and then because of the stronger stability of the tetrahedral intermediate.

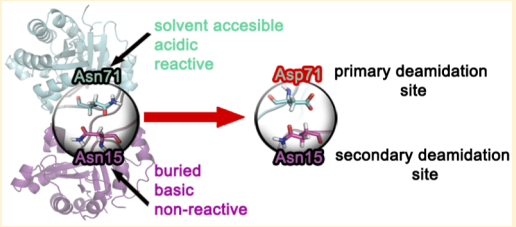

Deamidation of asparagine (Asn) is the reversible conversion of a neutral amide side chain to a negatively charged carboxylic acid, yielding an aspartic acid residue (Asp). This conversion in the amino acid sequence causes destabilization of peptide structures, which enhances chemical degradation of peptides and limits the lifetime of proteins.[1] The rate of deamidation of asparagine is mostly dependent on the primary structure of the peptides, and the reaction with an asparagine-glycine (Gly) sequence is known to be the most rapid conversion.[2] Under physiological conditions, deamidation occurs via a succinimide intermediate, and this formation is the rate-determining step of the overall reaction (Scheme 1).[3,4] As shown in the schematic representation of the suggested mechanism (Scheme 1), the formation of the succinimide intermediate is initiated by deprotonation of the backbone amide nitrogen of glycine [asn-gly(−)].

The nucleophilic attack of the backbone nitrogen on the asparagine side chain produces a metastable cyclic tetrahedral intermediate (tet). This intermediate is protonated, resulting in the release of one ammonia molecule. This step generates a relatively stable succinimide (suc) intermediate that is converted to asparagine (asp-gly) in further hydrolysis. Because of the biological importance of the deamidation reaction, there have been several studies dedicated to elucidating the details of the mentioned mechanism.[5−12] All of these studies concluded that the reaction should start via the removal of the glycine backbone amide hydrogen. In addition, Catak et al.[11] emphasized the importance of solvation in deamidation, demonstrating that water assistance enhances this phenomenon. This observation is in agreement with the experimental results showing that deamidation is prevented in low-water concentration media.[13]

Capasso et al. proved that the reaction mechanism of deamidation bears the same features in small peptides and in proteins.[14] However, it is known that it occurs much faster in peptides than in proteins.[1] Besides, there is a wide range of deamidation half-lives of several proteins that exhibit the same primary structure.[15]

In the study presented here, deamidation in the enzyme triosephosphate isomerase (TPI) is investigated. It has been proposed that deamidation in TPI regulates protein turnover, based on the fact that it is controlled by catalytic activity and

Received: June 30, 2014
Revised: January 10, 2015
Published: January 20, 2015

DOI: 10.1021/bi5008047
Biochemistry 2015, 54, 1429−1439

Scheme 1. Suggested Deamidation Mechanism of Capasso and Co-Workers under Physiological Conditions (pH 7.4)[3,4]

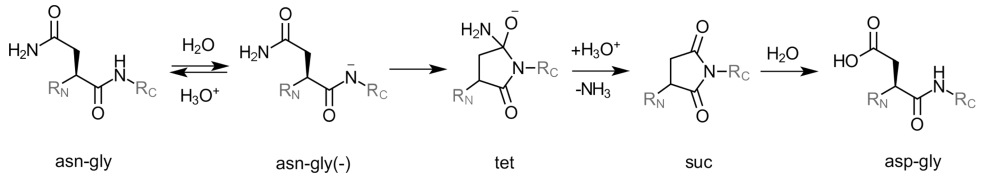

that it causes protein degradation.[1] Two distinct asparagines were found to be unstable under physiological conditions in each monomer of the homodimeric TPI: Asn15 and Asn71.[1,16] It has been suggested that deamidation in TPI occurs in a sequential order in a way that deamidation of Asn71 triggers Asn15 deamidation.[1] This interrelated deamidation in TPI allows us to compare the significance of desolvation, backbone acidity, and flexibility on this reaction. The special features of deamidation in TPI can be summarized as follows.

(1) In mammalian TPI, deamidation occurs at MetAsn15GlyArg and ThrAsn71GlyAla, which are located at the interdigitating loops (loop 1 and loop 3, respectively) of the two identical monomers of this homodimeric enzyme.[16]

(2) ThrAsn71GlyAla deamidates earlier than MetAsn15GlyArg, with the relative ratios of deamidated products [Asp71:Asp15] being 2.54:1 for human TPI and 1.73:1 for rabbit TPI.[16] Asn71 and Asn15 are depicted as primary (1°) and secondary (2°) deamidation sites in TPI, respectively.

(3) The *in vitro* half-life of the deamidation reaction in mammalian TPI was found to be 37.8 days (in 0.05 M phosphate at pH 7.0 and 37 °C).[1] Under the same conditions, the half-life of a small peptide is found to be 1.04 days.

(4) Mammalian TPI is active only as a dimer. There are four deamidation sites in an active homodimeric TPI, and they are located in a way that Asn71Gly (1° deamidation site) of one monomer is juxtaposed to Asn15Gly (2° deamidation site) of the other monomer, and vice versa (Figure 1).

(5) The rate of deamidation of Asn71 is enhanced by the increased catalytic activity of mammalian TPI.[16]

(6) Deamidation in TPI follows the general base catalysis mechanism.[16]

(7) It has been proposed that deamidated Asn71 [Asp71] would be a prerequisite for Asn15 deamidation.[17] However,

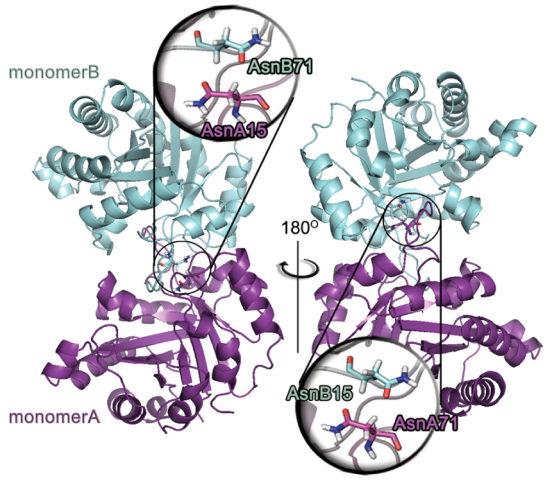

Figure 1. Location of Asn71 (1° deamidation site) and Asn15 (2° deamidation site) on the mammalian TPI crystal structure (Protein Data Bank entry 1R2R[23]).

Robinson et al. computed the deamidation coefficient (C_D) of Asp71:Asp15 (2.27:1),[18] which is in agreement with the experimental characterization of the TPI deamidation (2.54:1 for human TPI and 1.73:1 for rabbit TPI). Considering the fact that C_D values are calculated on crystal structures (i.e., on structures without any deamidation), it has been suggested that these two deamidations can also be considered as independent events.[1]

Robinson et al.[1] made an extensive review of deamidation and suggested several factors that would control the deamidation rate. Among these factors, the following are crucial for the different deamidation rates of the distinct Asn's under the same conditions:[1] (1) the intrinsic acidity of the involved nitrogen (i.e., the nitrogen atom of the backbone neighboring residue), (2) peptide steric hindrance that would control the formation of the tetrahedral intermediate, and (3) the leaving group probability of the tetrahedral intermediate.

In our previous study,[19] in which the initiation of deamidation in triosephosphate isomerase (TPI) has been investigated by molecular dynamics, it has been suggested that the global desolvation generated by the secondary structure would affect the deamidation rate. The effect of global desolvation on the rate of deamidation can be explained first by its relevance with acidity and flexibility. As the degree of desolvation increases, the acidity of the backbone amide and the flexibility of the amino acid would decrease.[19,20] Second, more desolvated residues would have less water in their first hydration shell, which would diminish the rate of deamidation considering the enhancing effect of water in deamidation.

Here, apo mammalian TPI was simulated by classical force field and molecular dynamics (MD) techniques to improve our understanding of the higher reactivity in Asn71 deamidation. The different reactivities of Asn15 and Asn71 in mammalian TPI were elucidated by considering the rate-determining factors mentioned above.[1] To investigate these factors, several descriptors were determined and applied to the MD trajectories. MD simulations were performed up to 1.5 μs using cuda-enabled graphics processing units (GPUs). To the best of our knowledge, these simulations are the longest MD simulations performed on TPI.

The kinetics of tetrahedral formation was also elucidated for both deamidation sites of TPI using QM/MM−MD with the umbrella sampling technique. To explain the slower rate in TPI, asparagine dipeptide is also modeled with the same protocol used for TPI. Because it has been shown with extensive experimental[1,21] and computational studies[10,11,22] that succinimide formation is the rate-determining step of the overall deamidation reaction and that succinimide formation is controlled by the rate of tetrahedral intermediate formation, this work focuses on tetrahedral formation only.

COMPUTATIONAL METHODS

Preparation of the Sample. The mammalian TPI structure was extracted from a rabbit TPI crystal structure

DOI: 10.1021/bi5008047
Biochemistry 2015, 54, 1429−1439

(Protein Data Bank entry 1R2R, 1.5 Å resolution[23]). This protein consists of two identical monomers that are differentiated by the conformation of their active sites. The monomers are labeled as monomers A and B, and this nomenclature is used to distinguish the amino acids located on either of these monomers (AsnA71, GlyB72, etc.).

The system was hydrogenated following a validation of the protonation states of the charged side chains with PROPKA,[20,24−26] and histidine residues were protonated according to their polar environment. The tleap module of AMBER12[27] was used to build topology and coordinate files. The system was solvated with explicit TIP3P[28] water molecules, resulting in cubic boxes with an edge length of 93.13 Å. Using a locally developed python script (see the Supporting Information), water molecules were added around the protein to obtain an initial density of 1.0 g/cm^3. The system contains ∼24000 water molecules (for a total of ∼80000 atoms). This corresponds to a protein concentration in the box of approximately half that of the original TPI crystal.

Molecular Dynamics Simulations. The simulations were performed using the AMBER12[27] program package with the pmemd module, and the cuda-enabled graphics processing units (GPUs) version of pmemd was used[29,30] for the production runs. All the simulations were performed using the ff03[31] and TIP3P[28] force field parameters for the protein and the water molecules, respectively. Periodic boundary conditions were applied, and an *NVT* ensemble was used with Andersen[32] temperature coupling. The particle mesh ewald (PME)[33] method was used to calculate long-range electrostatic interactions beyond a cutoff distance of 8 Å. Only the bonds involving hydrogen atom were constrained with the SHAKE[34] algorithm. The time step was 2 fs for both equilibration and production. The equilibrations were conducted in five stages. (1) To provide a proper geometry of the hydrogen atoms, all the heavy atoms, including water oxygen, were restrained with a harmonic potential of 50 kcal mol^{-1} Å^{-2} for 100.0 ps, at 10 K. (2) The same potential was applied for an additional 100.0 ps, but with removal of the restraint on the water oxygens to ensure optimized positions of water with respect to the protein environment. (3) This last step was repeated by decreasing the harmonic potential to 5 kcal mol^{-1} Å^{-2} for 100.0 ps. (4) The potential was removed for an additional 100.0 ps at 10 K to equilibrate the whole system. (5) The system was gradually heated to 300 K for 2000.0 ps. The velocities were randomly updated every 10 steps for equilibration stages 1−4 and every 100 for stage 5. The production runs were performed for 1.5 μs with velocities updated every 1000 steps.

Umbrella Sampling Calculations. *Preparation of the Systems Prior to QM/MM−MD Calculations.* The asparagine dipeptide was solvated with TIP3P[28] water molecules to result in a cubic system with edges of 55.8 Å, containing 5763 water molecules. Topology and coordinate files of this system were prepared with the tleap module of the AMBER12 program package,[27] and equilibration was performed using the same protocol as for the TPI sample.

For TPI structures, three frames were extracted from molecular dynamics trajectories. The criteria for extracting the structures are discussed in the relevant section. These structures consist of approximately 80000 atoms. Because of the large dimensions of the system, stochastic boundary conditions were applied.[35] A sphere with a radius of 20 Å from the center of mass of Asn15 and Asn71 was chosen to form the reaction region, and atoms 20−26 Å form the buffer region. The rest of the system was excluded by replacing the exterior protein residues with *N*-methylamide and acetamide. A harmonic restraint with a 20 kcal mol^{-1} Å^{-2} force constant was applied to atoms of both protein and water in the buffer region.

To obtain comparative results with the asparagine dipeptide, the water box of this system was also truncated with the same range defined for TPI (i.e., buffer region 20−26 Å from the center of mass of the solute).

Construction of the Reaction Coordinates. The conversion of asparagine to the tetrahedral intermediate with the umbrella sampling technique was investigated with a two-dimensional potential of mean force (PMF). The N−H deprotonation is described by one reaction coordinate (RC1) that is defined as the antisymmetric combination of distances d_1 and d_2 (Figure 2). The distance between the glycine backbone N and the side chain C (d_3 in Figure 2) was chosen as the second reaction coordinate (RC2).

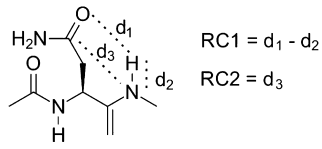

Figure 2. Definition of the reaction coordinates used to model the formation of the tetrahedral intermediate (tet) from asparagine (asn).

QM/MM−MD Calculations. In the case of the asparagine dipeptide, the solute and the water molecules are defined as the QM and the MM parts of the system, respectively (Figure 3a shows the QM part of the asparagine dipeptide). For TPI, the QM part contains Asn and Gly residues of the corresponding deamidation site (e.g., for the 1° and 2° deamidation site Asn71Gly72 and Asn15Gly16 belong to the QM region, respectively). Because the neighboring residues of either Asn or Gly are different for the 1° [ThrAsn71GlyAla] and 2° deamidation [MetAsn15GlyArg] sites, the QM part is limited to only Asn-Gly, to obtain a consistent comparison of the energetics between these two deamidation sites. Therefore, the effect of the neighboring atoms is included as an MM perturbation (e.g., van der Waals and electrostatics interactions) of the QM wave functions. In addition to the reactive Asn and Gly residues, four additional atoms from the N-terminal and C-terminal residues of Asn and Gly were included in the QM region to define the link atoms properly (i.e., to include the peptide bonds that link the deamidation region to its neighboring amino acids). The resulting QM part of TPI

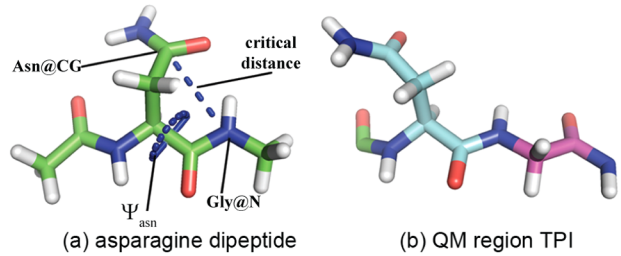

Figure 3. Representative figures for (a) the asparagine dipeptide and (b) the QM region of TPI. Asparagine and glycine residues are colored cyan and magenta, respectively, in panel b.

DOI: 10.1021/bi5008047
Biochemistry 2015, 54, 1429−1439

consists of 27 reactive atoms, including two link atoms (Figure 3b).

The effect of the QM size in our QM/MM−MD calculations is validated by including an additional amino acid in the QM part of one of the model systems studied here (see the Supporting Information for the details and results).

QM/MM−MD simulations were performed using the AMBER12[27] program package with the SANDER module. The MM region of TPI [protein and water atoms within 26 Å of the center of mass of the QM part (see above)] was treated with ff03 force field parameters.[31] The QM part was treated by SCC-DFTB for the calculations of the peptide in explicit water and TPI. SCC-DFTB has been chosen following a benchmark study of several approximated QM methods, including recent semiemprical Hamiltonians (see the Supporting Information for the computational details and the results of this analysis).

The window size was defined as 0.10 Å, yielding a total of 852 windows within the range of [RC1:RC2] = [−2.0, 1.0:1.5, 3.5]. To control the reaction coordinates, a harmonic potential centered on each window was applied with a force constant of 300 kcal mol^{-1} Å^{-2}. Each window was simulated during 15 ps with a time step of 0.5 fs. The results were analyzed using WHAM[36] to obtain the PMF of the corresponding mechanisms.

RESULTS

Stability of the Simulations. The root-mean-square deviations (rmsd's) of the Cα atom of (1) the dimer, (2) each monomer, and (3) α helices and β sheets of each monomer were monitored along the simulation with respect to the reference crystal structure. The deviations are more noticeable considering the rmsd of the dimer, compared to the deviations in the separated monomers (Figure 4). This

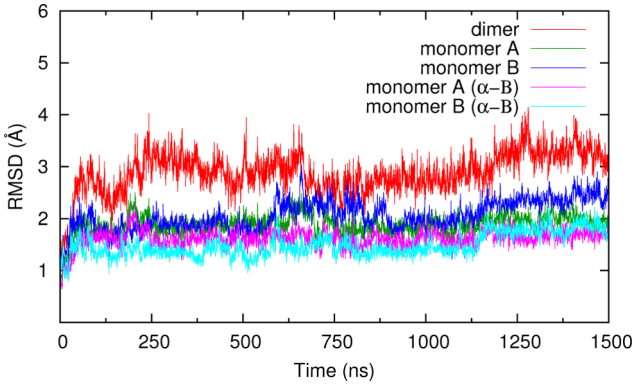

Figure 4. rmsd fluctuations along the molecular dynamics trajectory with respect to the crystallographic structure of each system. rmsd's are computed for the complete dimer structure (red), monomer A only (green), monomer B only (blue), all α helices and β sheets of subunit A (magenta), and all α helices and β sheets of subunit B (cyan).

result correlates with our previous molecular dynamics simulation analysis of six different TPI structures on a shorter time scale (60−90 ns).[19] The correlated motions of the monomers in the dimeric TPI enzyme, which was previously observed,[37] explain the rather high rmsd values of the dimer. On the other hand, deviations of each monomer hold a low rmsd value along the trajectory at 2.0−2.5 Å (Figure 4). Combining these remarks, we can conclude that our simulation is stable.

Solvent Accessibility. As demonstrated previously, "global desolvation ($N_{15.5\ Å}$)" can be used as an efficient descriptor to investigate the solvent accessibility of the amino acids of interest.[19] This descriptor was introduced by Li et al.[20] to predict the pK_a shift with respect to the global desolvation of amino acids in a protein environment, and it has been implemented in the previous versions of PROPKA.[20,24,26] Global desolvation analysis for both the Asn side chain and the Gly backbone was performed following the same protocol used in our previous study[19] and will not be detailed here.

$N_{15.5\ Å}$ of the Asn side chain of all of the deamidation sites was monitored along the simulation time (Figure 5), and the

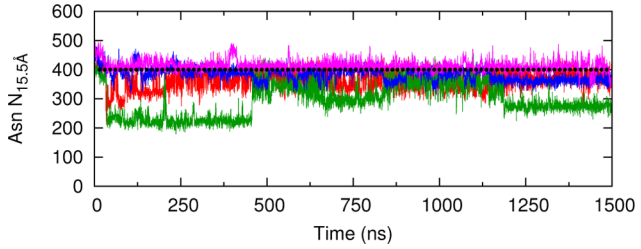

Figure 5. $N_{15.5\ Å}$ of the Asn side chain with respect to time (AsnA15, -A71, -B15, and -B71 are colored blue, red, magenta, and green, respectively).

Asn side chain desolvation with respect to the Gly backbone desolvation was plotted (Figure 6). To gain insights into

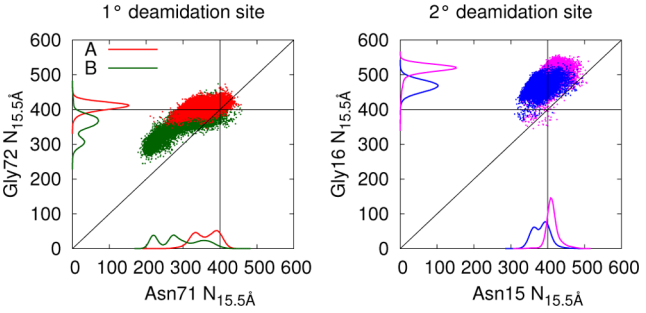

Figure 6. $N_{15.5\ Å}$ of the Asn side chain vs $N_{15.5\ Å}$ of the Gly backbone. Red and green points represent the 1° deamidation sites of monomers A and B, respectively. Blue and magenta points represent the 2° deamidation sites of monomers A and B, respectively. The probability distribution of $N_{15.5\ Å}$ of each deamidation site is shown with the corresponding colors.

populations of solvated residues along the simulation time, frames with Asn or Gly with $N_{15.5\ Å}$ values of <400 (i.e., the cutoff for solvation as suggested by Li et al.[20]) were identified and considered to be solvated. The number of frames having solvated residues was summed and divided by the total number of frames in the simulation to obtain the percent occurrence of "$N_{15.5\ Å}$ < 400" (Table 1).

Side chains of Asn in the 1° deamidation site on both monomers go to the solvated state at the beginning of the simulation (Figure 5). They stay solvated along the simulation (Figure 6), resulting in percent occurrences of "$N_{15.5\ Å}$ < 400" equal to 84.7 and 98.0% for monomers A and B, respectively (Table 1). Backbones of GlyA and GlyB in the 1° deamidation site have probabilities of 19.0 and 96.2%, respectively, to be solvated.

DOI: 10.1021/bi5008047
Biochemistry 2015, 54, 1429−1439

Table 1. Percent Occurrence of Solvated Conformations of Asn and Gly in 1° and 2° Deamidation Sites (DSs) of Monomers A and B

	1° DS		2° DS	
	Asn71	Gly72	Asn15	Gly16
		$N_{15.5\ Å} < 400$		
A	84.7	19.0	74.4	0.4
B	98.0	96.2	15.3	0.4
		$N_{15.5\ Å} < 420$		
A	97.8	77.6	94.3	1.0
B	99.7	98.6	71.4	0.7

In the 2° deamidation site, AsnA and AsnB are solvated over 74.4 and 15.3% of the simulation, respectively. GlyA and GlyB of the 2° deamidation site always stay buried along the simulation (Figure 6) with probability to be solvated almost zero (Table 1).

The difference in percent solvation of Asn in the 2° deamidation site on monomer A (74.4%) and B (15.3%) is notable. A similar difference can be observed for Gly in the 1° deamidation site with the solvation values: 19.0% for GlyA72 and 96.2% for GlyB72. The question that arises from these results is whether this large gap between the same residue on different monomers is a realistic picture indicating a strongly different behavior of the two monomers, or whether it is just a matter of the way of defining the descriptor of solvation. From Figure 6, it can be seen that both GlyA72 (a, red, *y*-axis) and AsnB15 (b, magenta, *x*-axis) gather on the border of the solvation limit (400). The solvation limit of 400 has been chosen to describe the global desolvation of residues as it is proposed by Li et al. However, considering the observed specific characteristics of TPI, here we suggest to use 420 as a limit to define solvated and desolvated frames. The updated solvation probabilities ("$N_{15.5\ Å} < 420$") of GlyA72 and AsnB15 are 77.6 and 71.4%, respectively, which are much closer to their counterparts in other monomers [98.6% for GlyB72 and 94.3% for AsnA15 (Table 1)]. Choosing either 400 or 420 as a limit of desolvation does not change the overall trend of solvation, which can be summarized as follows.

(1) Asn residues in the 1° deamidation site on both of the monomers are always solvated along the simulation.

(2) Gly residues in the 1° deamidation site are also solvated but have probabilities smaller than those of their Asn neighbors.

(3) Asn residue in the 2° deamidation site are solvated but less so than Asn residue in the 1° deamidation site.

(4) Gly residue in the 2° deamidation site always stay buried.

Backbone Amide Acidity. Radkiewicz et al.[5] showed that the acidity of the Gly backbone amide hydrogen is highly correlated with the peptide conformation by calculating the relative proton affinity of *N*-formyl-glycinamide as a function of the Ramachandran plot (Φ and Ψ angles) (HF/6-31+G*//HF/3-21G).

In this study, the relative proton affinity (PA) and the change in Gibbs free energy in aqueous media (ΔG_{aq}) of 2-acetamido-*N*-methylacetamide [M1 (Scheme 2)] were calculated using a higher optimization scheme (see the Supporting Information for the computational details).

The deviations of PA and ΔG_{aq} with respect to the Ramachandran plot of 2-acetamido-*N*-methylacetamide are given in Figure 7. In accordance with those of Radkiewicz et al., our results suggest that (1) the PA (or ΔG_{aq}) of the Gly backbone amide deviates up to ∼24 kcal/mol (or ∼17 kcal/mol) with respect to changes in backbone conformation, (2) the acidity decreases going from region I to III (Figure 7), and (3) either the PA or ΔG_{aq} is mainly dependent on the Ψ angle rather than Φ.

Scheme 2. Model Peptides for QM Calculations without (M1) or with (M2) an Asparagine Side Chain[a]

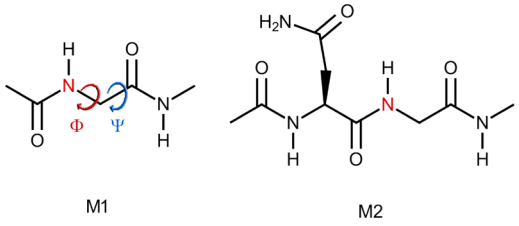

[a]The backbone amide nitrogen is colored red. Φ and Ψ dihedrals are shown on M1 only.

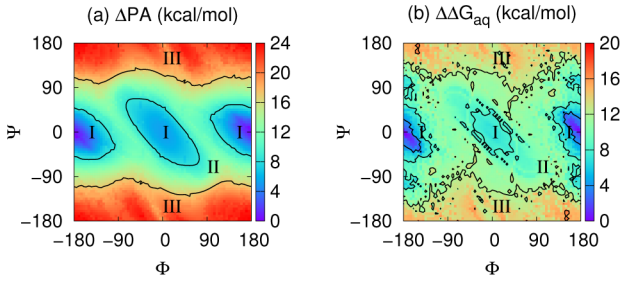

Figure 7. Correlation of the acidity of the amide backbone hydrogen of model M1 as a function of the Ramachandran plot at the B3LYP/6-31+G level of theory. Contour lines divide the surfaces into three regions with increments of 8 and 5.6 kcal/mol in energy difference for ΔPA and $\Delta\Delta G_{aq}$, respectively. Aqueous phase calculations are conducted with CPCM. The relative proton affinity (ΔPA) and $\Delta\Delta G_{aq}$ increase upon going from blue to red as the acidity decreases.

The accuracy of the PA and ΔG_{aq} analysis obtained by model M1 (Scheme 2) has been validated using a larger model, which contains an asparagine residue as an addition to model M1 [model M2 (Scheme 2)]. The results corresponding to this larger model also describe the most acidic conformations in region I and the most basic ones in region III (see the Supporting Information for the computational details and for the results).

Radkiewicz et al.[5] used the strong relationship between the conformation and backbone amide acidity to explain the relative ease of deamidation in peptides that have Gly next to Asn, compared to other neighboring amino acids.[5] They concluded that[5] the extra flexibility of glycine allows the system to occupy more acidic conformations and consequently increases the rate of deamidation. Here we investigate if the same correlation can also be used to explain the different rates of Asn15Gly and Asn71Gly in TPI, because the flexibility of glycine will be limited within a protein and might be different in the primary and secondary structures of the protein (i.e., Asn15Gly and Asn71Gly are located on loop 1 and loop 3 in TPI, respectively).

The Ramachandran plots of the Gly backbone were plotted within the simulation time. Gly of the 1° deamidation site mostly populates region I or the border between regions I and II (Figure 8), which corresponds to the most acidic conformation of glycine with respect to the ΔPA and $\Delta\Delta G_{aq}$ results (Figure 7), whereas Gly of the 2° deamidation site occupies region III and some parts of region II that are closer to

DOI: 10.1021/bi5008047
Biochemistry 2015, 54, 1429−1439

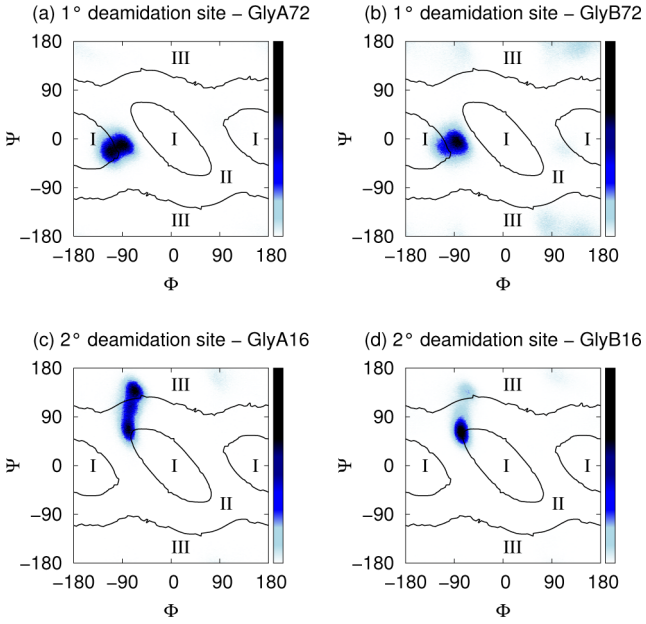

Figure 8. Probability distribution of Φ and Ψ dihedrals of (a) GlyA72, (b) GlyB72, (c) GlyA16, and (d) GlyB16. The probability increases from white to black.

region III (Figure 8). These fields are less acidic than the regions occupied by Gly of the 1° deamidation site.

The variations of conformations in the Ramachandran plot with respect to time for the 1° deamidation site are shown in Figure 9. Conformations at the border of region I and II are

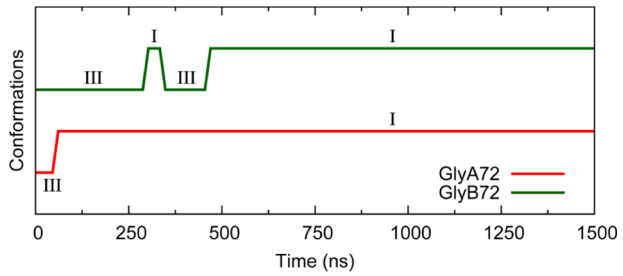

Figure 9. Changes of conformations in the Ramachandran plot[8] with respect to time.

classified as in region I for the sake of simplicity. The most acidic conformation I is observed after 32 ns for GlyA72, and this conformation remains until the end of the simulation (1500 ns) (Figure 9). On the other hand, for GlyB72, clustering on the most acidic conformation (region I) does not occur before 289 ns (Figure 9). This geometry is occupied for only 40 ns, and then the system goes back to a basic conformation for an additional 130 ns. The most probable conformation of this residue (region I) is filled starting from 462 ns to the end of the simulation (Figure 9). The fluctuations are less significant for the 2° deamidation site of TPI, because all GlyA16 and GlyB16 invade a much more narrow area on the Ramachandran plot compared to GlyA72 and GlyB72 (data not shown).

To gain insights into stabilizing factors of the more acidic and more basic conformations, hydrogen bond analysis is performed. The analysis showed that the 2° deamidation site, for both A and B monomers, is engaged in strong protein interactions more significant than the 1° one (see Figure 10 and

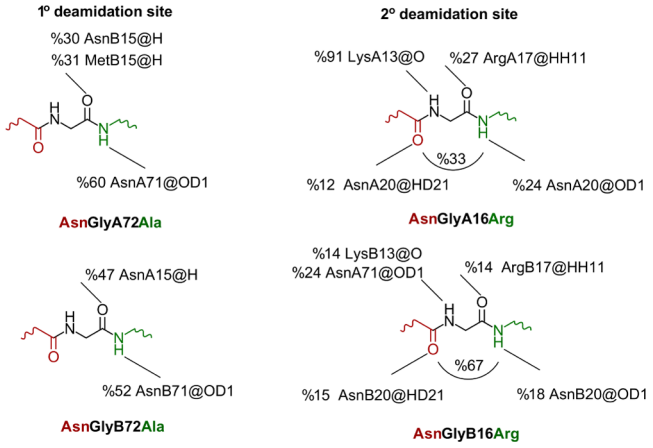

Figure 10. Hydrogen bond network of the 1° and the 2° deamidation sites. The percent occupancies of hydrogen bonds between Asn@O (or Gly@H, Gly@O, or Ala/Arg@H) and protein atoms are given. Asn, Gly, and Ala/Arg are colored red, black, and green, respectively.

the Supporting Information for the details). In addition, the 2° deamidation site is rigidified by the intramonomeric interactions that might be the stabilizing effect of more basic conformations in the 2° deamidation site of TPI.

Near Attack Conformations (NAC's). One of the main hypotheses that explains the diminishing rate of deamidation in proteins with respect to small peptides is that the loss of flexibility would prohibit the required orientation of Asn and Gly to deamidate. To accomplish deamidation, the peptide backbone should rotate freely.[1] In addition, the distance between Gly@N and Asn@CG (Figure 3) should be small enough to produce a cyclic intermediate via a nucleophilic attack.[10,11] Here, this critical distance was determined to be 3.5 Å in accordance with previous QM studies.[10,11] Again in these studies, the Asn Ψ dihedral (Ψ_{asn}) of the reactive conformation was defined to be ∼185° (Figure 3). Considering the dynamical behavior of our systems, we have chosen to define the most favorable dihedral for tetrahedral formation in the range of Ψ_{asn} [110°:260°] that corresponds to the widest range around Ψ_{asn} = 185°. The trajectories were analyzed, and the geometries that meet those two criteria were classified as near attack conformers (NAC's), as generally described in the literature. The importance of NAC formation in obtaining biologically relevant reaction rates has been previously shown.[38]

The probabilities of finding NAC's within the whole simulation are listed in Table 2. The 1° deamidation site

Table 2. Percent Occurrences of Near Attack Conformers (Gly@N-Asn@CG distance of <3.5 Å, +110.0° ≤ Ψ_{asn} ≤ +260.0°)

	residue 71A	residue 71B	residue 15A	residue 15B
NAC percentage	67.2	45.0	1.5	3.1

holds the geometrical features susceptible to deamidation almost half or more of the simulation with percent occurrence values of 67.2 and 45.0% in monomers A and B, respectively. On the other hand, NAC's rarely occur in the 2° deamidation site of TPI (1.5 and 3.1% for monomers A and B, respectively). Figure 11 shows the representative structures of the 1° and the 2° deamidation sites of TPI, including the most frequently observed dihedrals and hydrogen bond interactions. As discussed above, the 2° deamidation site is involved in a strong

DOI: 10.1021/bi5008047
Biochemistry 2015, 54, 1429−1439

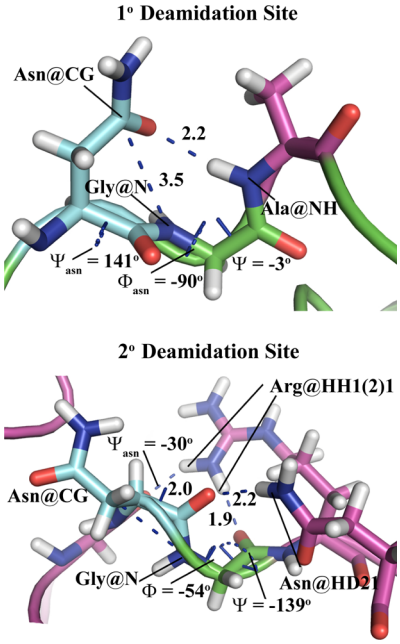

Figure 11. Representative structures of the 1° and 2° deamidation sites showing the most frequently observed interactions and dihedrals. Asn, Gly, and the rest of the peptide are colored cyan, green, and purple, respectively.

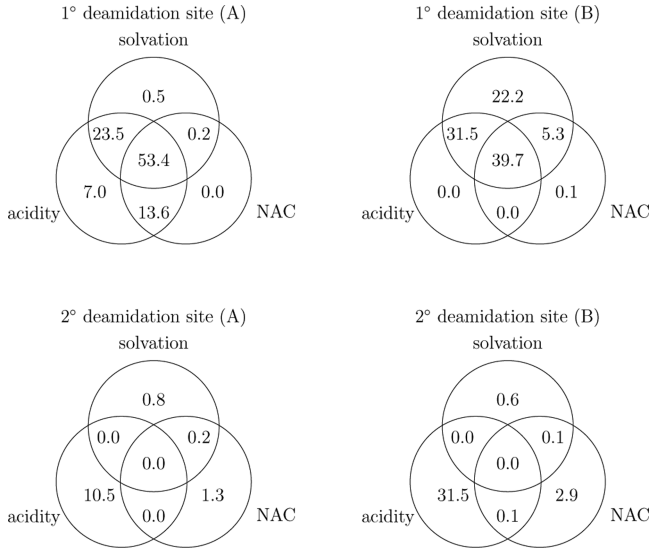

Figure 12. Percent occurrences of solvation, glycine backbone amide acidity, and NAC.

hydrogen bond network. The correlation between this hydrogen bonding pattern and the geometrical features of the Asn15Gly16 residues can be seen from Figure 11. Combining hydrogen bond and NAC analysis results with Figure 11, we can conclude that this network stabilizes the 2° deamidation site of TPI in a geometry that disfavors tetrahedral formation.

Comprehensive Results. Up to this point, differentiations in terms of global desolvation, acidity, and NAC analysis of TPI were introduced. Global desolvation and peptide conformation−acidity analysis determine the intrinsic acidity of the glycine backbone amide, and the NAC analysis measures the conformational availability for tetrahedral formation. As stated by Robinson et al.,[1] "the properly aligned side chain (NAC) reacts only if deprotonation has occured prior to alignment". Hence, the correspondence among these conditions should be evaluated. This is accomplished by analyzing if these events (solvation, acidity, and NAC) are observed within the same frame or different frames during the simulation time (see the Supporting Information for the definition of each descriptor, solvation, acidity, and NAC).

For the 1° deamidation site of mammalian TPI, the probabilities of being both solvated, acidic, and resembling NAC (solvation ∩ acidity ∩ NAC) are 53.4 and 39.7% for monomers A and B, respectively (Figure 12). In the case of the 2° deamidation site of TPI, there are no frame that meets these criteria in the same frame, returning 0 probability in the intercept (Figure 12).

For the 2° deamidation site of TPI, in which the solvation probabilities are almost 0, acidic conformations of GlyA and GlyB are observed as 10.5% (A) and 31.6% (B). The 1° deamidation site A of TPI also has a considerably large amount of acidic conformations in unsolvated areas {total 20.6% → [acidity/(solvation ∩ NAC)] + [(acidity ∩ NAC)/solvation] = 7.0% + 13.6% = 20.6%}. These results indicate that Gly might have the acidic conformations, although it is buried inside the protein and its flexibility is limited by intermolecular interactions.

To test the reliability of our results, the same analysis was performed on the first 1 μs of our simulations (see the Supporting Information for the results). The trend of the distribution of the frames is found to be the same for the analysis on either 1 μs (Supporting Information) or 1.5 μs (Figure 12), revealing that our simulations can be considered as converged.

Kinetic Aspects: Free Energy Calculations. In Backbone Amide Acidity, we have proposed that Asn71 should deamidate faster than Asn15 because the NH group of Gly72 deprotonates easier, so that the reaction would be initiated faster. Here, this claim has been tested with free energy calculations using QM/MM tools with the umbrella sampling technique. The statistics on the Ramachandran plots obtained in that section were used to refine the possible frames that will be subject to umbrella sampling calculations. This approach allows us to combine the classical statistics with the kinetic results. The refinement is accomplished by extracting snapshots from the regions where Gly16 and Gly72 have the highest probability to be found in the Ramachandran plot according to our MD statistics (Figure 8). As disscussed above, these regions correspond to more acidic and less acidic regions for Asn71Gly72 [region I (Figure 8)] and Asn15Gly16 [region III (Figure 8)], respectively. These structures are labeled as C1-A (Asn71Gly72) and C2 (Asn15Gly16).

For the QM/MM−MD calculations, the reactive parts of the models (residues treated by QM) are defined as Asn71Gly72 and Asn15Gly16 for models C1-A and C2, respectively. To make a more decent comparison of the glycine amide acidity, an additional snapshot is extracted from the Ramachandran plot of Asn71Gly72 (C1-B). The geometrical features of this snapshot correspond to a less acidic conformation of Gly72 [region III (Figure 8)]. To gain deeper insights into the effect of high-order structure on the rate of tetrahedral formation, the asparagine dipeptide is also included in the model. Considering the computational expense, the simulations were performed within the region [RC1:RC2] = [−2.0, 1.0:1.5, 3.5]. Within this region, the initial geometry [RC1, RC2 = (1.0, 3.5)] corresponds to the NAC for all of the models.

DOI: 10.1021/bi5008047
Biochemistry 2015, 54, 1429−1439

The formation of the tetrahedral intermediate occurs via a concerted mechanism for all three models [C1-A, C1-B, and C2 (Figure 13)]. The first-order saddle point was detected around

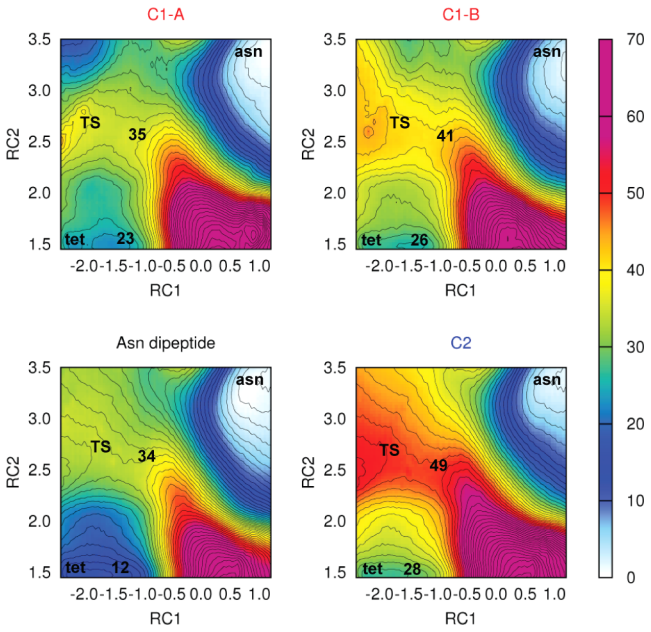

Figure 13. Free energy profile for the tetrahedral (tet) formation from asparagine (asn) in TPI for models C1-A, C1-B, and C2 (SCC-DFTB/MM−MD). Energetics are given in kilocalories per mole (the counter level is 1.5 kcal/mol). Regions having free energy values of >70 kcal/mol use the color of 70 kcal/mol.

(RC1, RC2) = (−1.5 Å, 2.5 Å), revealing a late transition state as suggested in previous DFT calculations[10,11] and the calculations performed in the study present here (see the Supporting Information).

For models C1-A and C1-B, the energy barriers are found at ∼35 and ∼41 kcal/mol, respectively, indicating that the reaction barrier increases with decreasing acidity (see the Supporting Information for the details).

For model C2, although the TS is located approximately in the same region and shows geometrical features similar to those of either of the models of the 1° deamidation site (see the Supporting Information for the details), the activation barrier is ∼14 and ∼8 kcal/mol higher than those of models C1-A and C1-B, respectively. The relative energies of the tetrahedral intermediate (tet) are ∼23, ∼26, and ∼28 kcal/mol for C1-A, C1-B, and C2, respectively. The stabilization of the tet is in accordance with Hammond's postulate as the relative energy of the product increases with an increase in the barrier.[39]

In the Supporting Information, the representative frames of the transition states for three of the models are given. In all cases (C1-A, C1-B, and C2), it can be seen that no residue within 5 Å of the Gly backbone nitrogen has strong attractive (or repulsive) interactions with the deamidation site.

A comparison with the asparagine dipeptide shows that the barriers of the more acidic conformation (C1-A) and the asparagine dipeptide are isoenergetic (∼34 and ∼35 kcal/mol, respectively). On the other hand, the less acidic conformation of the 1° deamidation site (C1-B) has a barrier 6 kcal/mol higher than that of the asparagine dipeptide. The tetrahedral intermediate is approximately 11 and 14 kcal/mol less stabilized the asparagine dipeptide for C1-A and C1-B, respectively. For the 2° deamidation site, the barrier is 14 kcal/mol higher than the barrier found for the asparagine dipeptide, and the tetrahedral intermediate is approximately 16 kcal/mol less stabilized.

DISCUSSION

Why Does Asn71 Deamidate Faster Than Asn15 in Mammalian TPI? To explain the relatively rapid reaction in the 1° deamidation site of TPI, global desolvation, backbone amide acidity, and near attack conformer analysis were performed for Asn15Gly16 and Asn71Gly72. According to global desolvation analysis, the 1° deamidation site is more solvated than the 2° deamidation site (Figure 6), showing that the former would be exposed to water more frequently than the latter. This result would explain the faster reaction at the 1° deamidation site, considering the enhancing effect of water on deamidation.[11]

The more significant result obtained from global desolvation analysis is the great difference between the desolvation of Gly16 and Gly72. Although Gly72 might be solvated more than half of the simulation, Gly16 is always buried (desolvated) (Scheme 1 and Table 1). The greater value of desolvation on Gly16 would lead to a higher pK_a in the backbone amide. The higher pK_a of the 2° deamidation site will cause the shift of the AsnGly ↔ AsnGly(−) equilibrium in Figure 1 to the reactant side (AsnGly). As a result of the decrease in the amount of activated Gly [asngly(−)], initiation of deamidation would be prohibited.

In addition to global desolvation, a more local view of the glycine backbone amide acidity (Backbone Amide Acidity) was also examined by its correlation with backbone conformations (Ramachandran plot). This analysis showed that the 1° deamidation site has a greater probability of being found in the most acidic regions (region I) of the Ramachandran plot compared to the 2° deamidation site (Figure 8). Thus, Gly amide of the 2° deamidation site would be less acidic than the 1° deamidation site. Hence, via combination of both global and local effects, the deprotonation of the Gly amide would require a greater energy in the case of the 2° deamidation site.

To test this hypothesis, free energy calculations were performed on two deamidation sites of mammalian TPI using QM/MM tools. The activation barrier of the less acidic conformation (C1-B) is found to be 6 kcal/mol higher than that of the more acidic one (C1-A) (Figure 13). In addition, model C2 in which tetrahedral formation is modeled at the secondary deamidation site has a barrier 14 kcal/mol higher than that of model C1-A. This model also represents a less acidic structure of Gly16 with respect to the backbone conformations. Combining these facts, we can conclude that the acidity of the backbone amide has a crucial impact on the initiation of the deamidation reaction.

In the deamidation reaction, deprotonation of the Gly amide is followed by the formation of a cyclic tetrahedral intermediate (Scheme 1). The energy required to form this cyclic intermediate would be diminished by the increased possibility of bearing conformers that resemble the transition state geometry (NAC). The percent occurrence of near attack conformers (NAC's) was found to be around 50% in the case of the 1° deamidation site (Table 2). NAC's were almost never observed in the 2° deamidation site, affirming that the formation of a tetrahedral intermediate would be much slower than that of the 1° deamidation site.

Via combination of the remarks on glycine amide acidity and probability of having near attack conformers, it can be

DOI: 10.1021/bi5008047
Biochemistry 2015, 54, 1429−1439

concluded that both deprotonation and cyclization steps require more energy in the case of Asn15 deamidation than in the case of Asn71 deamidation.

Up to this point, the deamidation reaction was analyzed by discriminated steps (i.e., deprotonation, tetrahedral intermediate formation). To achieve a successful reaction, the neighboring Gly should be acidic enough (considering both local and global factors), and at the same time, geometries should resemble NAC's. In the 1° deamidation site, these three descriptors were observed at the same time almost half of the frames of the simulation (see Figure 12, top). In the case of the 2° deamidation site, the probability of being found in these three states is zero (see Figure 12, bottom). This result indicates that under the same conditions, almost half of the geometries of the 1° deamidation site can initiate deamidation, whereas none of the geometries in the 2° deamidation site are reactive.

Why Is the Half-Life of the Small Asn Peptide Smaller Than That of TPI? Under the same experimental conditions, the deamidation half-lives of a small peptide and TPI are found to be 1.04 and 37.8 days, respectively. Previous studies suggest that the slower rate of deamidation in proteins compared to those of their small counterparts might be caused by the less acidic character of the neighboring residue or by the lower flexibility in proteins.[1,7,11] The lower flexibility could be related to them being located on more rigid conformations (e.g., α helices). On the other hand, deamidation sites that exhibit a less rigid secondary structure conformation (i.e., loops) could also be stabilized by strong hydrogen bond networks. All of these proposals point out that deamidation rates of small peptides and proteins would be discriminated in the initiation step.

In this study, the initial step of deamidation is modeled in the asparagine dipeptide to mimic a small peptide and consequently to compare its kinetics with those of TPI. Both Asn71 and Asn15 are located on flexible loops of TPI; this fact eliminates the possible effect of a more complex secondary structure (i.e., α helices). In addition, no special interactions that would hinder the formation of a tetrahedral intermediate were found (see Figure 4 of the Supporting Information). Hence the comparison between the asparagine dipeptide and the models from TPI focuses on only the relative acidity of the glycine backbone amide.

Models C1-B and C2 have activation barriers (41 and 49 kcal/mol, respectively) higher than that of the asparagine dipeptide (34 kcal/mol). Only model C1-A has an approximately isoenergetic barrier (35 kcal/mol) with the asparagine dipeptide. The initial structures of C1-B and C2 are relatively less acidic than that of C1-A. Thus, if the geometrical features allow the TPI deamidation site to be acidic enough, the forward barrier (asn → tet) would be as small as the small peptide. These results are in agreement with the proposals that suggest that deamidation would be slower in proteins because of the diminished acidity of the glycine amide.

On the other hand, more crucial differences between the kinetics of the small peptide and TPI arise in the stabilization of the tetrahedral intermediate. This intermediate is more than ∼10 kcal/mol less stabilized for any of the models of TPI than the asparagine dipeptide. The tetrahedral intermediate is a five-membered heterocyclic compound. The relatively less stable intermediate in the case of TPI might be explained by the higher strain energy introduced by the long peptide chain in TPI. This result indicates that the barrier of reverse reaction (tet → asn) is much smaller for TPI than it is for the small peptide. Hence, the slower rate in TPI compared to that of its smaller counterpart stems not only from the weaker reactivity (i.e., higher forward barrier) but also from the poorer stability of the tetrahedral intermediate (i.e., lower backward barrier).

Tertiary Structure Effect. The analysis of global desolvation along the simulation can shed light on the effect of the tertiary structure on different rates of deamidation. As shown previously,[19] the higher solvation values for the 1° deamidation site can be explained by the relative flexibility of loop 3 on which Asn71Gly is located, compared to loop 1 involving Asn15Gly.

Primary Structure Effect. Most of the studies in the literature, related to the primary structure effect on deamidation, focus on the residues in the C-terminal (n + 1) or N-terminal (n − 1) position with respect to Asn. In these studies, n + 1 residues are found to be the most crucial factors affecting the deamidation rates, while the effects of n − 1 residues are found to be negligible.[1,40] Despite the observed changes in rates of pentapeptides bearing different n + 2 residues,[1] there are not enough studies that sufficiently explain its impact on deamidation. In mammalian TPI, AsnGly is followed by Ala and Arg in the 1° and 2° deamidation sites, respectively. Hydrogen bond analysis of this study indicates that both of the Asn residues are stabilized by their n + 2 residues (see the Supporting Information). The hydrogen bond between the Ala backbone amide and the Asn side chain in the 1° deamidation site favors the formation of near attack conformations (Figure 11). On the other hand, the stable interaction between the Asn and Arg backbone in the 2° deamidation site limits the Φ and Ψ rotations; therefore, the probability of being found in the relatively more acidic regions is diminished. These results illustrate that the n + 2 residue may favor or disfavor the initiation of deamidation. Hence, we suggest that the effect of the n + 2 residue should be included in further formulations of the deamidation rate prediction.

CONCLUSIONS

We have explored the different reactivities of two deamidation sites in the enzyme TPI using microsecond MD simulations. The formation of the tetrahedral intermediate was modeled using the umbrella sampling technique with QM/MM−MD tools. Three descriptors were introduced to analyze the deamidation reaction: (i) global desolvation, (ii) backbone amide acidity, and (iii) near attack conformer analysis. These independent descriptors were efficiently used to gain insights into the sequential deamidation process in mammalian TPI. According to these analyses, the initiation of deamidation would be facilitated at Asn71 because of its greater degree of solvation and also because of the higher acidity of the adjacent glycine (Gly72) backbone amide. With respect to the results obtained from near attack conformer analysis, the initiation would be faster in the case of Asn71 and tetrahedral formation would require less energy. Combining these outcomes, we can conclude that deamidation at Asn15 is hindered by both global and local factors.

The tetrahedral intermediate formation was also modeled with asparagine dipeptide to compare the kinetics with the two different deamidation sites in TPI. The most significant difference between the deamidation rates of TPI and the small peptide appears to be the stabilization of the tetrahedral intermediate. The tetrahedral intermediate is more than 10 kcal/mol less stabilized in TPI than in the asparagine dipeptide.

DOI: 10.1021/bi5008047
Biochemistry 2015, 54, 1429−1439

To the best of our knowledge, these are the first kinetic results that relate the diminishing effect of the high-order structure with the stability of the intermediate in the deamidation reaction.

Our findings also contribute to the understanding of the impact of the peptide sequence on the deamidation rate. The global desolvation analysis points to the importance of tertiary structure on deamidation. The backbone acidity and the near attack conformation results highlight the possible role of residues $n + 2$ to Asn.

■ ASSOCIATED CONTENT

Supporting Information

Complementary details about the computational methodology (i.e., solvation process and QM/MM modeling of the formation of the tetrahedral intermediate), semiempirical and SCC-DFTB benchmark study, and comprehensive results for the first microsecond of the molecular dynamics simulation. This material is available free of charge via the Internet at http://pubs.acs.org.

■ AUTHOR INFORMATION

Corresponding Author

*E-mail: gerald.monard@univ-lorraine.fr. Phone: +33 (0) 383.684.381. Fax: +33 (0)383.684.371.

Funding

I.U. acknowledges a joint Ph.D. grant from the TUBITAK Joint Ph.D. Program (2214-B). Part of this work was possible because of access to the HPC resources of CINES (Centre Informatique National de l'Enseignement Superieur) under an HPC-EUROPA2 allocation in September 2012, made by GENCI (Grand Equipement National de Calcul Intensif).

Notes

The authors declare no competing financial interest.

■ REFERENCES

(1) Robinson, N. E., and Robinson, A. B. (2004) *Molecular Clocks: Deamidation of Asparaginyl and Glutaminyl Residues in Peptides and Proteins*, Althouse Press, Cave Junction, OR.

(2) Robinson, A. B., Scotchler, J. W., and McKerrow, J. H. (1973) Rates of Nonenzymic Deamidation of Glutaminyl and Asparaginyl Residues in Pentapeptides. *J. Am. Chem. Soc. 95*, 8156−8159.

(3) Capasso, S., Mazzarella, L., Sica, F., and Zagari, A. (1989) Deamidation via Cyclic Imide in Asparaginyl Peptides. *Pept. Res. 2*, 195−200.

(4) Capasso, S., Mazzarella, L., Sica, F., Zagari, A., and Salvadori, S. (1993) Kinetics and Mechanism of Succinimide Ring Formation in the Deamidation Process of Asparagine Residues. *J. Chem. Soc., Perkin Trans. 2*, 679−682.

(5) Radkiewicz, J. L., Zipse, H., Clarke, S., and Houk, K. N. (1996) Accelerated Racemization of Aspartic Acid and Asparagine Residues via Succinimide Intermediates: An ab Initio Theoretical Exploration of Mechanism. *J. Am. Chem. Soc. 118*, 9148−9155.

(6) Kosky, A. A., Razzaq, U. O., Treuheit, M. J., and Brems, D. N. (1999) The Effects of α-helix on the Stability of Asn Residues: Deamidation Rates in Peptides of Varying Helicity. *Protein Sci. 8*, 2519−2523.

(7) Radkiewicz, J. L., Zipse, H., Clarke, S., and Houk, K. N. (2001) Neighboring side chain effects on asparaginyl and aspartyl degradation: An ab initio study of the relationship between peptide conformation and backbone NH acidity. *J. Am. Chem. Soc. 123*, 3499−3506.

(8) Konuklar, F. A. S., Aviyente, V., Monard, G., and Ruiz Lopez, M. F. (2004) Theoretical Approach to the Wear and Tear Mechanism in Triosephoshate Isomerase: A QM/MM Study. *J. Phys. Chem. B 108*, 3925−3934.

(9) Peters, B., and Bernhardt, L. (2006) Asparagine deamidation: pH-dependent mechanism from density functional theory. *Biochemistry 45*, 5384−5392.

(10) Catak, S., Monard, G., Aviyente, V., and Ruiz-López, M. F. (2006) Reaction Mechanism of Deamidation of Asparaginyl Residues in Peptides: Effect of Solvent Molecules. *J. Phys. Chem. A 110*, 8354−8365.

(11) Catak, S., Monard, G., Aviyente, V., and Ruiz-Lopez, M. F. (2009) Deamidation of Asparagine Residues: Direct Hydrolysis versus Succinimide-Mediated Deamidation Mechanisms. *J. Phys. Chem. A 113*, 1111−1120.

(12) Takahashi, O., Kobayashi, K., and Oda, A. (2010) Modeling the Enolization of Succinimide Derivatives, a Key Step of Racemization of Aspartic Acid Residues: Importance of a Two-H_2O Mechanism. *Chem. Biodiversity 7*, 1349−1356.

(13) Garza-Ramos, G., Tuena de Gomez-Puyou, M., Gomez-Puyou, A., Yuksel, K. U., and Gracy, R. W. (1994) Deamidation of Triosephosphate Isomerase in Reverse Micelles: Effects of Water on Catalysis and Molecular Wear and Tear. *Biochemistry 33*, 6960−6965.

(14) Capasso, S., and Salvadori, S. (1999) Effect of the Three-Dimensional Structure on the Deamidation Reaction of Ribonuclease A. *J. Pept. Res. 54*, 377−382.

(15) Robinson, N. E. (2002) Protein deamidation. *Proc. Natl. Acad. Sci. U.S.A. 99*, 5283−5288.

(16) Yüksel, K., and Gracy, R. W. (1986) In vitro deamidation of human triosephosphate isomerase. *Arch. Biochem. Biophys. 248*, 452−459.

(17) Gracy, R. W., and Yuan, P. M. (1980) Spontaneous deamidation of two asparagines within the subunit contact sites of human triosephosphate isomerase. *Fed. Proc. 39*, 1690.

(18) Robinson, N. E., and Robinson, A. B. (2001) Prediction of protein deamidation rates from primary and three-dimensional structure. *Proc. Natl. Acad. Sci. U.S.A. 98*, 4367−4372.

(19) Ugur, I., Aviyente, V., and Monard, G. (2012) Initiation of the Reaction of Deamidation in Triosephosphate Isomerase: Investigations by Means of Molecular Dynamics Simulations. *J. Phys. Chem. B 116*, 6288−6301.

(20) Li, H., Robertson, A. D., and Jensen, J. H. (2005) Very Fast Empirical Prediction and Rationalization of Protein pK_a Values. *Proteins 61*, 704−721.

(21) Capasso, S., Mazzarella, L., Kirby, A. J., and Salvadori, S. (1996) Succinimide-mediated pathway for peptide bond cleavage: Kinetic study on an Asn-Sar containing peptide. *Pept. Sci. 40*, 543−551.

(22) Konuklar, F. A. S., Aviyente, V., Sen, T. Z., and Bahar, I. (2001) Modeling the Deamidation of Asparagine Residues via Succinimide Intermediates. *J. Mol. Model. 7*, 147−160.

(23) Aparicio, R., Ferreira, S. T., and Polikarpov, I. (2003) Closed Conformation of the Active Site Loop of Rabbit Muscle Triosephosphate Isomerase in the Absence of Substrate: Evidence of Conformational Heterogeneity. *J. Mol. Biol. 334*, 1023−1041.

(24) Bas, D. C., Rogers, D. M., and Jensen, J. H. (2008) Very Fast Prediction and Rationalization of pK_a Values for Protein−Ligand Complexes. *Proteins 73*, 765−783.

(25) Olsson, M. H. M., Søndergard, C. R., Rostkowski, M., and Jensen, J. H. (2011) PROPKA3: Consistent Treatment of Internal and Surface Residues in Empirical pK_a predictions. *J. Chem. Theory Comput. 7*, 525−537.

(26) Søndergaard, C. R., Olsson, M. H., Rostkowski, M., and Jensen, J. H. (2011) Improved treatment of ligands and coupling effects in empirical calculation and rationalization of pK_a values. *J. Chem. Theory Comput. 7*, 2284−2295.

(27) Case, D. A., Darden, T. A., Cheatham, T. E., III, Simmerling, C. L., Wang, J., Duke, R. E., Luo, R., Walker, R. C., Zhang, W., Merz, K. M., Roberts, B., Hayik, S., Roitberg, A., Seabra, G., Swails, J., Goetz, A. W., Kolossváry, I., Wong, K. F., Paesani, F., Vanicek, J., Wolf, R. M., Liu, J., Wu, X., Brozell, S. R., Steinbrecher, T., Gohlke, H., Cai, Q., Ye, X., Wang, J., Hseih, M.-J., Cui, G., Roe, D. R., Mathews, D. H., Seetin, M. G., Salomon-Ferrer, R., Sagui, C., Babin, V., Luchko, T., Gusarov,

DOI: 10.1021/bi5008047
Biochemistry 2015, 54, 1429−1439

S., Kovalenko, A., and Kollman, P. A. (2012) *AMBER 12*,, University of California, San Francisco.
(28) Jorgensen, W. L., Chandrasekhar, J., Madura, J. D., Impey, R. W., and Klein, M. L. (1983) Comparison of simple potential functions for simulating liquid water. *J. Chem. Phys. 79*, 926−935.
(29) Götz, A. W., Williamson, M. J., Xu, D., Poole, D., Le Grand, S., and Walker, R. C. (2012) Routine microsecond molecular dynamics simulations with AMBER on GPUs. 1. Generalized born. *J. Chem. Theory Comput. 8*, 1542−1555.
(30) Salomon-Ferrer, R., Götz, A. W., Poole, D., Le Grand, S., and Walker, R. C. (2013) Routine Microsecond Molecular Dynamics Simulations with AMBER on GPUs. 2. Explicit Solvent Particle Mesh Ewald. *J. Chem. Theory Comput. 9*, 3878−3888.
(31) Duan, Y., Wu, C., Chowdhury, S., Lee, M. C., Xiong, G., Zhang, W., Yang, R., Cieplak, P., Luo, R., Lee, T., Caldwell, J., Wang, J., and Kollman, P. (2003) A Point-Charge Force Field for Molecular Mechanics Simulations of Proteins Based on Condensed-Phase Quantum Mechanical Calculations. *J. Comput. Chem. 24*, 1999−2012.
(32) Andersen, H. C. (1980) Molecular Dynamics Simulations at Constant Pressure and/or Temperature. *J. Chem. Phys. 72*, 2384−2394.
(33) Essmann, U., Perera, L., Berkowitz, M. L., Darden, T., Lee, H., and Pedersen, L. G. (1995) A Smooth Particle Mesh Ewald Method. *J. Chem. Phys. 103*, 8577−8593.
(34) Ryckaert, J.-P., Ciccotti, G., and Berendsen, H. J. (1977) Numerical Integration of the Cartesian Equations of Motion of a System with Constraints: Molecular Dynamics of n-alkanes. *J. Comput. Phys. 23*, 327−341.
(35) Brooks, C. L., and Karplus, M. (1983) Deformable Stochastic Boundaries in Molecular Dynamics. *J. Chem. Phys. 79*, 6312−6325.
(36) Grossfield, A. *WHAM: The weighted histogram analysis method*, version 2.0.9, University of Rochester Medical Center, Rochester, NY.
(37) Cansu, S., and Doruker, P. (2008) Dimerization affects collective dynamics of triosephosphate isomerase. *Biochemistry 47*, 1358−1368.
(38) Hur, S., and Bruice, T. C. (2003) Just a near attack conformer for catalysis (chorismate to prephenate rearrangements in water, antibody, enzymes, and their mutants). *J. Am. Chem. Soc. 125*, 10540−10542.
(39) Hammond, G. S. (1955) A Correlation of Reaction Rates. *J. Am. Chem. Soc. 77*, 334−338.
(40) Wakankar, A. A., and Borchardt, R. T. (2006) Formulation Considerations for Proteins Susceptible to Asparagine Deamidation and Aspartate Isomerization. *J. Pharm. Sci. 95*, 2321−2336.

DOI: 10.1021/bi5008047
Biochemistry 2015, 54, 1429−1439